Progress in Structural Elucidation of Glasses by ^{27}Al and ^{11}B Satellite Transition NMR Spectroscopy

G. Kunath-Fandrei[1], D. Ehrt[2], and C. Jäger[3]

[1] Friedrich-Schiller-Universität Jena, PATF, Max-Wien-Platz 1, D-07743 Jena
[2] Friedrich-Schiller-Universität Jena, Chemische Fakultät, Otto-Schott-Institut, Fraunhoferstr. 6, D-07743 Jena
[3] Max-Planck-Institut für Polymerforschung, Postfach 31 48, D-55021 Mainz

Z. Naturforsch. **50a**, 413–422 (1995); received December 16, 1994

Dedicated to Prof. Dr. W. Müller-Warmuth on the occasion of his 65th birthday

The structure of $Na_2O-Al_2O_3-B_2O_3$ and $Na_2O-Al_2O_3-P_2O_5$ glasses with 70 mole% B_2O_3 or P_2O_5 and varied Na/Al ratio is investigated using standard ^{31}P MAS NMR and ^{27}Al and ^{11}B Satellite Transition NMR spectroscopy. The role of the two network formers on the glass structure is discussed. For the AlO_x units and BO_3 and BO_4 groups both chemical shifts and quadrupole interaction parameters including their distribution widths are reported. Besides this, the advantages of Satellite Transition spectroscopy are demonstrated both for ^{27}Al and ^{11}B NMR.

Key words: NMR, Glass, Structure, Satellite Transition, ^{11}B, ^{27}Al, ^{31}P.

1. Introduction

Nuclear Magnetic Resonance is one of the most versatile spectroscopic techniques for probing the microstructure of disordered solids (for reviews see e.g. [1]). In contrast to X-ray diffraction and optical spectroscopy, NMR does not require three-dimensional translational symmetry of a unit cell of any material to obtain reasonably narrow resonances. Especially ^{29}Si and ^{31}P MAS NMR (MAS: Magic Angle Sample Spinning) offers the opportunity to obtain reliable quantitative numbers of the distributions of silicon phosphorus over the various Q^n units (n: number of bridging oxygen atoms between like SiO_4 or PO_4 units [2]) forming the network of a glass. Hence, MAS NMR has been applied to a variety of different glass systems and ceramics, investigating e.g. the influence of different sorts of cations on the microstructure of the material or checking the applicability of binary or random modified network models of the distributions of the Q^n groups [i.e. 1, 3–8].

Besides this, so-called quadrupole nuclei (spin I larger than 1/2) play an important role in NMR of glasses because most of the NMR active nuclei are indeed quadrupole nuclei. Particularly, the important nuclei ^{27}Al ($I = 5/2$) and ^{11}B ($I = 3/2$) possess an electric quadrupole momentum. Hence, in most cases the NMR spectra are broadened by quadrupolar effects [3]. That this is not necessarily a disadvantage has been proven by Bray and coworkers in the early days of NMR on glasses [e.g. 9]. They have shown that the trigonal and tetrahedrally coordinated boron can easily be distinguished by ^{11}B NMR, since only the BO_3 spectra are broadened by second order quadrupolar effects, whereas the quadrupole interaction in the BO_4 units is rather negligible compared with the dipolar broadening. The situation is different for ^{27}Al NMR since the second order broadening is always severe and masks the small differences in the chemical shifts of differently coordinated Al species. Only MAS offers the opportunity to discriminate between the various AlO_x units ($x = 4, 5, 6$) [e.g. 11], but quantification of the spectra in terms of the relative occupancy is extremely difficult if not impossible in many cases.

Recently, Satellite Transition (ST) Spectroscopy has been proposed as a powerful tool for elucidating the microstructure of disordered solids [12]. The observation of the MAS spinning sidebands of the inner ST ($\pm 3/2 \leftrightarrow \pm 1/2$) of any $I = 5/2$ nucleus such as ^{27}Al offers an important advantage over the Central Transition (CT) MAS pattern: Second order quadrupolar broadening is reduced by a factor of 3.4 simply by a lucky combination of the spin number I and the value of m (transition $\pm m \leftrightarrow (m-1)$). We have made extensive use of this additional line narrowing both in crystalline, disordered and partially crystallized solids

Reprint requests to Dr. C. Jäger.

0932-0784 / 95 / 0400-0413 $ 06.00 © – Verlag der Zeitschrift für Naturforschung, D-72027 Tübingen

Dieses Werk wurde im Jahr 2013 vom Verlag Zeitschrift für Naturforschung in Zusammenarbeit mit der Max-Planck-Gesellschaft zur Förderung der Wissenschaften e.V. digitalisiert und unter folgender Lizenz veröffentlicht: Creative Commons Namensnennung-Keine Bearbeitung 3.0 Deutschland Lizenz.

This work has been digitalized and published in 2013 by Verlag Zeitschrift für Naturforschung in cooperation with the Max Planck Society for the Advancement of Science under a Creative Commons Attribution-NoDerivs 3.0 Germany License.

Zum 01.01.2015 ist eine Anpassung der Lizenzbedingungen (Entfall der Creative Commons Lizenzbedingung „Keine Bearbeitung") beabsichtigt, um eine Nachnutzung auch im Rahmen zukünftiger wissenschaftlicher Nutzungsformen zu ermöglichen.

On 01.01.2015 it is planned to change the License Conditions (the removal of the Creative Commons License condition "no derivative works"). This is to allow reuse in the area of future scientific usage.

[12–20]. The important point is, that the quadrupolar broadening of those spinning sidebands is suppressed to such a degree, that the limit of spectral resolution in disordered solids is achieved (governed by isotropic chemical shift distributions which cannot be reduced further by sample rotation). Simultaneously, the quadrupole parameters are not lost since they can be recovered from the intensities of the ST MAS spinning sidebands, which allows in turn the determination of all parameters including their distribution widths [12, 16]. Also, the quadrupole interaction and chemical shifts have been determined in various polycrystalline solids and applications to ^{7}Li, ^{17}O, ^{23}Na, ^{27}Al and ^{51}V have been published [21–30].

It is the aim of this paper to demonstrate the opportunities of Satellite Transition (ST) Spectroscopy both for ^{27}Al and ^{11}B NMR for various glasses and crystallized samples of the systems Na_2O–Al_2O_3–P_2O_5 and Na_2O–Al_2O_3–B_2O_3. One interesting question concerns the structural changes when replacing the glass former P_2O_5 by B_2O_3 in these glasses; but rather than discussing this in very detail we would show and discuss the advantages of ^{27}Al Satellite Transition (ST) NMR results for probing the structure of glasses.

On the other hand we show that ^{11}B ST spectroscopy leads to interesting results, too. Our work is an extention of recent papers suggesting ^{11}B ST spectroscopy as a sensitive tool to monitor chemical shift changes of both BO_3 and BO_4 units as function of the glass composition [31]. Besides this we use ^{11}B ST NMR spectroscopy to determine the quadrupole interactions for both borate units including their distributions widths and will show, that this kind of spectroscopy raises the question what disorder in amorphous solids means. We have found in our systems completely different sizes of the distributions of the quadrupole interaction for BO_3 and BO_4. We also discuss the opportunity of detecting different BO_3 units via the ST MAS sidebands and compare this with recent approaches using 2D DAS NMR [32] and NQR [e.g. 33].

2. Experimental Details

2.1. Glass Preparation and Analysis

Three different phosphate glasses NAP (Na_2O–Al_2O_3–P_2O_5) have been melted in covered SiO_2 crucibles at 1300 °C. $NaH_2PO_4 \cdot H_2O$, $Al(PO_3)_3$ and P_2O_5 (all of optical quality) were used as raw materials. The raw materials for the borate glasses NAB (Na_2O–Al_2O_3–B_2O_3) were Na_2CO_3, H_3BO_3 and $Al(OH)_3$ (again of optical quality). These glasses were melted in covered Pt crucibles at 1300 °C. In both glass systems the content of the corresponding network formers B_2O_3 and P_2O_5 were constant (70 mole%), whereas the ratio Na_2O/Al_2O_3 was 2, 1 and 1/2 (see also Table 1 and 2).

Table 1. Characterization of the glasses (composition, refractive index n_e, Abbe-number ν_e, density ϱ and detected crystal phases after tempering at 650 °C for 24 hours. Two kinds of $Al(PO_3)_3$ modifications, one cubic (c) and one hexagonal (h) (ASTM 13-430 and 15-364) and at the highest Al_2O_3 content of 20 mole% two $AlPO_4$ modifications (trydimite T and crystobalite C, ASTM 20-44 and 11-500) were found.

	NAP 10 (mole%)	NAP 15 (mole%)	NAP 20 (mole%)
Al_2O_3	10	15	20
Na_2O	20	15	10
P_2O_5	70	70	70
n_e	1.5125	1.5140	1.5240
ν_e	68.5	68.6	69.5
ϱ (g/cm^3)	2.550	2.580	2.608
crystal phases (X-ray)	$Al(PO_3)_3$-c $Al(PO_3)_3$-h	$Al(PO_3)_3$-c $Al(PO_3)_3$-h	$Al(PO_3)_3$-c $AlPO_4$-T $AlPO_4$-C

The melts were poured into preheated moulds and annealed at temperatures slightly above the glass temperature T_g. The cooling rate was 10 K/h. The castings were selectively cut, ground and polished into different sample shapes for various investigations. The refractive index has been measured using a Pulfrich refractometer. The densities of the glasses have been determined by measuring the buoyancy of polished glass samples in alcohol using Archimedes' principle. The glass transition temperatures T_g and the crystallization temperatures T_k were measured by thermal analysis DTA using powder samples. Furthermore the samples have been tempered at the maximum of their crystallization rate at 650 °C for 24 hours to investigate the crystallization behaviour. These samples have also been characterized by X-ray diffraction.

2.3. NMR

The ^{27}Al ST MAS NMR spectra have been acquired on a Bruker AMX 400 spectrometer supplemented with a high power transmitter operating at 104.26 MHz and a Bruker highspeed MAS probe. Extremely short pulses (0.8 ... 1.0 μs) have been used be-

ing equivalent to a pulse angle of about 15°. Repetition times differed between 100 ms and 400 ms. No saturation effects have been observed using these repetition times. The MAS spinning frequencies were varied between 10 and 13 kHz to separate adjacent spinning sideband families completely and to allow an accurate cubic spline baseline correction [12]. The MAS frequency was stable within 3 Hz. Between 25000 and 100000 scans were accumulated. The sweep width was set to 2.5 MHz. 16 k data points were acquired and zero filled to 32 k prior to Fourier transformation. One on-resonance experiment and an off-resonance experiment at 400 kHz were carried out. The spectra were corrected and combined as described in [12].

^{31}P MAS NMR spectra were also obtained under MAS conditions at a field strength of 9.4 T corresponding to a resonance frequency of 161.98 MHz with spinning speeds of 10 to 12 kHz. The 90° pulse width was 2.7 μs. For the glassy samples repetition times of 300 s were necessary to avoid saturation effects. About 150 scans were accumulated. The thermally treated (recrystallized) samples were measured twice with repetition times of 300 s (no saturation) and 200 ms to observe the relaxation behaviour of expected different crystalline phases. The sweep width was set to 500 kHz, 8 k data points were acquired. The chemical shift is referenced against 85% solution of H_3PO_4.

^{11}B ST MAS spectra were recorded using both an ASX 500 and AMX 400 with high power transmitter operating at 160.46 and 128.38 MHz, respectively. Short pulses of 1.0 μs, MAS frequencies of 14 and 13 kHz, 16 k data points, and 10 s recycle time were used. About 1000 scans for the glass samples and for the recrystallized material were accumulated. The sweep width was again 2.5 MHz. Both on resonance and off-resonance (800 and 400 kHz) experiments were carried out and data processed as described for the ^{27}Al NMR spectra. The ^{11}B chemical shift is referenced against 1 molar H_3BO_3. The lineshape simulations have been described in detail in [16].

3. Results

3.1. Physical Chemical Properties

3.1.1. Na_2O–Al_2O_3–P_2O_5 glasses

As described earlier the P_2O_5 content of all three glasses was constant at 70 mole%. The compositions are summarized in Table 1. For all three compositions stable glasses were obtained without spontaneous crystallization. Table 1 also contains the values of the refractive index n_e and of the Abbe number v_e, of the density and of the crystal phases after thermal treatment of the glasses at 650 °C for 24 hours. The glass transition temperatures are 450 ... 490 °C and the temperature for the maxium of the crystallization rate is between 600 and 650 °C.

Table 2. Summary of the properties of the NAB glasses. For more details see text.

	NAB 10 (mole%)	NAB 15 (mole%)	NAB 20 (mole%)
Al_2O_3	10	15	20
Na_2O	20	15	10
B_2O_5	70	70	70
n_e	1.4946	1.4940	crystal phases
v_e	59.9	59.5	(X-ray)
ϱ (g/cm^3)	2.166	2.148	$9Al_2O_3 \cdot 2B_2O_3$
			$2Al_2O_3 \cdot B_2O_3$

3.1.2. Na_2O–Al_2O_3–B_2O_3 glasses

The sample compositions are listed in Table 2. In contrast to the NAP glasses the melt with the lowest Na_2O/Al_2O_3 ratio or vice versa the highest Al_2O_3 content of 20 mole% crystallized spontaneously. Using X-ray diffraction crystalline aluminium borate $9Al_2O_3 \cdot 2B_2O_3$ (orthorhombic, ASTM 32-2) has been determined as main crystal phase. Also orthorhombic $2Al_2O_3 \cdot B_2O_3$ has been found as a minor crystal phase (ASTM 9-158). This phase is also found in the other glasses after tempering at 650 °C for 24 hours.

In Table 2 selected properties of these glasses are summarized. The values for T_g were 430–470 C. The maximum of the crystallization rate was found between 560 and 680 °C.

3.2. NMR Results

3.2.1. Na_2O–Al_2O_3–P_2O_5 glasses

^{31}P-NMR spectra of the glass samples are shown in Figure 1. All NMR spectra of these glasses show a broad featureless MAS center band. The isotropic value of the chemical shift remains relatively constant at about 35 ppm irrespective of the glass composition with a half width at half height of about 20 ppm. However, there is a change in the intensities of the spinning sidebands. But this is not characteristic as

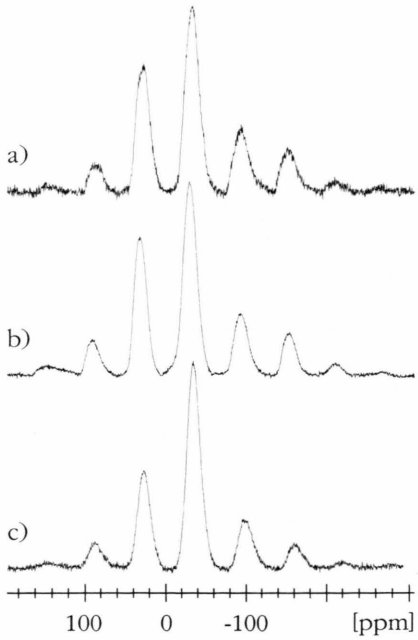

Fig. 1. ^{31}P MAS spectra of glass samples (a) NAP 10, (b) NAP 15 and (c) NAP 20. The NMR data and peak assignment are summarized in Table 3.

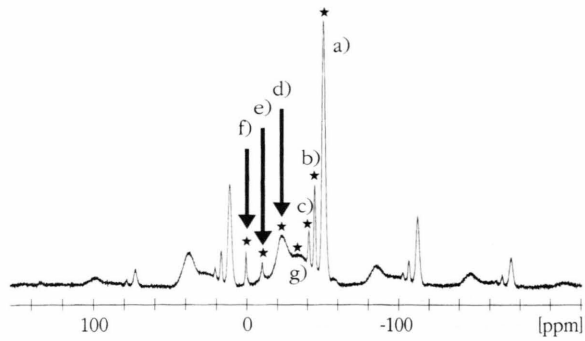

Fig. 2. ^{31}P MAS spectrum of the tempered sample NAP 10 at 9.4 T (a)–(g) assign the different sites in both the glass and the crystal phases. The chemical shift parameters and assignments are listed in Table 4.

Table 3. ^{31}P chemical shift parameters of the amorphous NAP samples. Chemical shifts are referenced against 85% solution of H_3PO_4.

	δ_{iso} [ppm]	$\Delta\nu$ [ppm]	$\Delta\delta$ [ppm]	η	I/I_{total} [%]	Comments
NAP 10	−36.0	22.0	−267	0.35	100	Q^2
NAP 15	−31.0	20.0	−272	0.26	100	Q^2
NAP 20	−35.0	20.0	−232	0.24	100	Q^2

function of the composition. Hence, we conclude that Q^2 groups dominate the ^{31}P MAS spectra in all three glasses. In order to prove a possible presence of Q^3 groups (at least for NAP 10) we repeated the experiments with extremely short (100 ms) and long (10 min) repetition times in order to exploit possible differences in the spin-lattice relaxation times of those units. But no change in the MAS sideband pattern was observed Also, a difference spectrum between the glasses NAP 10 and NAP 20 did not bring a significant hint for the presence of Q^3 groups. The chemical shift parameters extracted from a Herzfeld/Berger analysis [34] are listed in Table 3.

Additionally, we investigated tempered samples of NAP 10 as well as of NAP 20 (24 hours at 650 °C, maximum of crystallization rate). The ^{31}P spectrum of NAP 10 shows a complex structure (Figure 2). The central peaks are labeled with asterisks and the remaining peaks are the spinning sidebands (SSB). We can then distinguish seven different phosphorus sites. Three recrystallized phases with isotropic chemical shift values at −51, −45, and −41 ppm possess the typical SSB-behaviour of metaphosphates (sites, a, b, c, respectively). Site a) can clearly be assigned to aluminium metaphosphate [35]. Because of the X-ray data where a second $Al(PO_3)_3$ modification (hexagonal besides cubic) is detected, we assign site b) to the hexagonal modification. The assignment of the peak at about −41 ppm is not yet clear. Since the isotropic chemical shift of $NaPO_3$ is more positiv with about −23 ppm [35, 36], we attribute this line to a metaphosphate with mixed cations Al^{3+} and Na^+, but a definite assignment is not possible at the moment and requires further investigations. Besides this, two further narrow resonances are found without spinning sidebands (e, f) at −10.3 and +0.4 ppm which can be assigned to Q^0 units, obviously with mixed cations Na^+ and Al^{3+} for the line at −10.3 ppm and H_3PO_4. The occurrence of phosphoric acid is possible because of the extremely hygroscopic behaviour of the powdered glass sample with the lowest Al_2O_3 content. The line width at half height of these five resonances is about 1–2 ppm. Furthermore, two more resonances are observed with isotropic chemical shifts at −32 and −22.9 ppm and line widths of 27 and 7 ppm, respectively, which are certainly amorphous metaphosphates. The peak at about 23 ppm can be assigned to $NaPO_3$ [35, 36]; the

other one corresponds to the NMR signal of the glassy matrix. For the tempered NAP 20 glass (increased Al_2O_3 content) only four ^{31}P resonances are found. Besides the aluminium metaphosphate peak at about − 51 ppm and the broad resonance of the glass at − 36 ppm, the two cristobalite- and trydimite-like $AlPO_4$ modifications [35, 37, 39] are found in agreement with the X-ray data. All chemical shift parameters of the tempered samples are listed in Table 4.

The *^{27}Al MAS spectra* of all glass samples are shown in Figure 3. In the upper part the central transition (CT) MAS patterns are shown, whereas at the bottom several expanded ST MAS sidebands are presented for comparison in the same frequency scale. This clearly shows the improved resolution as explained in the Introduction. The isotropic value of the chemical shift was determined by comparing the CT and ST MAS patterns.

Table 4. ^{31}P chemical shift parameters of the tempered glasses NAP 10 and NAP 20.

Line	δ_{iso} [ppm]	$\Delta\nu$ [ppm]	$\Delta\delta$ [ppm]	η	I/I_{total} [%]	Comments
10-a)	−51.0	2.0	−180	0.50	27.4	$Al_4(P_4O_{12})$ [35]
b)	−45.1	1.5	−174	0.38	6.3	$Al(PO_3)_3$-h [35]
c)	−41.2	1.5	−143	0.08	2.0	Q^2, presumably
		error:	± 10	±0.1		mixed cations
g)	−32.9	27.0	?	?	44.9	glass matrix
d)	−22.9	7.0	−242	0.50	17.2	$NaPO_3$ [35, 36, 38] amorphous
e)	−10.3	1.5	?	?	0.8	Q^0 with mixed cations Na^+ and Al^{3+}
f)	+0.4	1.0	?	?	1.4	'H_3PO_4'
20-a)	−51.2	2.0	−182	0.52	26.1	$Al_4(P_4O_{12})_3$ [35]
b)	−31.3	1.5	?	?	3.6	$Al(PO_4)$-T [35, 39]
c)	−28.3	1.5	?	?	3.5	$Al(PO_4)$-C [35, 37, 39]
d)	−36.0	17.0	?	?	66.8	glass matrix

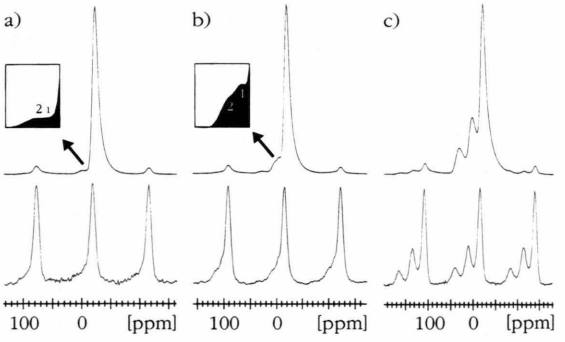

Fig. 3. ^{27}Al MAS spectra of glass samples (a) NAP 10, (b) NAP 15 and (c) NAP 20. The top part of the figure shows the CT region, whereas some ST MAS spinning sidebands are shown in the bottom part. 1) and 2) assign $Al(OAl)_6$ and $Al(OP)_5$ units, respectively.

The NAP 10 spectrum is dominated by a peak at about − 20 ppm with a correct isotropic shift value of − 10.8 ppm due to octahedrally coordinated Al with phosphorus in the second coordination shell [40–43]. Additionally, there is a small but broad peak left from the CT signal at about + 4 ppm. Because of the isotropic chemical shift this line can be assigned to pentacoordinated Al with phosphorus in the second coordination shell. With increasing Al_2O_3 content (NAP 15) a third resonance is found at about 0 ppm. It can be recognized in both the CT pattern (the right of the two small peaks) but more clearly as a distinct shoulder in the ST MAS sidebands which clearly shows the advantages of ST spectroscopy. The chemical shifts are + 2.2 and + 14.4 ppm and the lines are assigned to $Al(OAl)_6$ and $Al(OP)_5$, respectively. All parameters (chemical shift and quadrupole ineraction) are listed in Table 5. The values in parentheses should be considered with some caution since they are based on the CT analysis alone because of the low intensities of those lines. Both, the large line width of the signal at 2.2 ppm in NAP 10 and the comparison of that resonance with the CT of NAP 15 support the assumption, that in NAP 10 and NAP 15 this small resonance pattern is caused by the same two sites but with less $Al(OAl)_6$ as in NAP 10.

Finally, the Al_2O_3-richest sample NAP 20 shows three clearly resolved lines with the correct chemical shifts at − 11.2, + 13.1 and + 43.0 ppm. They belong to 4-, 5-, and 6-coordinated aluminium with phosphorus in the second coordination shell.

3.2.2. Na_2O–B_2O_3–Al_2O_3 glasses

The ^{27}Al MAS NMR spectra for the CT area are shown in Figure 4. As described earlier NAB 10 and 15 are completely amorphous whereas NAB 20 is spontaneously crystallized having $9\,Al_2O_3 \cdot 2\,B_2O_3$ as main crystal phase. The lineshape analysis is shown, too for the various resonances of the amorphous network parts. For NAB 10 mainly tetrahedrally coordinated Al is found with boron in the second coordination shell. In contrast to this 4-, 5- and 6-coordinated Al is detected in NAB 15 with dominating $Al(OB)_4$. The results (chemical shifts and quadrupole parameters) and assignments of the resonances are summarized in Table 6 (a) and (b). The lineshape analysis of the partially crystallized sample NAB 20 is

Table 5. ^{27}Al NMR results and peak assignment of NAP glasses. Shifts are referenced against aqueous solution of $AlCl_3$.

	δ_{iso} [ppm]	$\Delta\nu$ [Hz]	ν_Q [kHz]	$\Delta\nu_Q$ [kHz]	η	I/I_{total} [%]	Comment [40, 41]
NAP 10	−10.8	545	418	208	0.97	96.5	$Al(OP)_6$ $Al[(OP)_5–OA11]$
	(+ 4.0)	(1840)	(307)	(156)	(0.80)	3.5	$Al(OAl)_6/Al(OP)_5$
NAP 15	−10.7	601	380	290	0.89	83.3	$Al(OP)_6$ $Al[(OP)_5–OAl]$
	+ 2.2	(1160)	(655)	(271)	(0.30)	7.2	$Al(OAl)_6$
	+14.4	(1140)	(640)	(271)	(0.40)	9.5	$Al(OP)_5$
NAP 20	−11.2	573	514	292	0.49	51.9	$Al(OP)_6$ $Al[(OP)_5–OAl]$
	+13.1	898	606	490	0.35	32.0	$Al(OP)_5$
	+43.0	598	448	(400)	(0.71)	16.1	$Al(OP)_4$

Table 6. Summary of the ^{27}Al ST simulation parameters of NAB glasses.

	δ_{iso} [ppm]	$\Delta\nu$ [Hz]	ν_Q [kHz]	$\Delta\nu_Q$ [kHz]	η	I/I_{total} [%]	Comments [17, 42]
NAB 10	64.5	1080	770	195	0.50	93.6	$Al(OB)_4$ $Al[(OB_3)–OAl]$
	37.1	750	902	431	0.43	6.4	$Al(OB)_5$
NAB 15	63.5	1225	773	235	0.51	71.6	$Al(OB)_4$ $Al[(OB_3)–OAl]$
	37.1	828	903	431	0.26	25.1	$Al(OB)_5$
	11.3	508	792	104	0.44	3.3	$Al(OB)_6$
NAB 20	70.0		1360	0	0.43	10.3	AlO_4
$9Al_2O_3$	52.0		1080	0	0.00	11.9	$AlO_5(1)$
$2B_2O_3$	43.0		1420	0	0.49	11.4	$AlO_5(2)$
	8.0		910	0	0.44	18.1	AlO_6
glass matrix	61.1	1159	621	50	0.55	28.3	$Al(OB)_4$ $Al[(OB_3)–OAl]$
	38.1	855	645	50	0.25	15.6	$Al(OB)_5$
	12.5	1175	550	50	0.22	4.4	$Al(OB)_6$

easy. Recently, we have investigated polycrystalline $9Al_2O_3 \cdot 2B_2O_3$ by ^{27}Al MAS NMR spectroscopy [17]. The corresponding NMR spectrum is also shown in Fig. 4c for comparison with the ^{27}Al NMR spectrum of NAB 20. It is clear from this comparison, that only a part of the Al is contained in the crystal phase $9Al_2O_3 \cdot 2B_2O_3$. Neglecting the minor crystal phase $2Al_2O_3 \cdot B_2O_3$, the ^{27}Al NMR spectrum of the remaining glassy matrix can be obtained simply by subtracting the $9Al_2O_3 \cdot 2B_2O_3$ lineshape from the experimental 27Al MAS spectrum of NAB 20. The difference spectrum is shown in Figure 4d. There are several conclusions. First of all nearly 50% of the total Al content is now in the crystal phase, whereas the second half of the Al is 4-, 5- and 6-coordinated in the glassy matrix. Actually, the difference lineshape resembles the ^{27}Al NMR spectrum of NAB 15. The numbers for the Al content of the various structural units and the chemical shifts and quadrupole parameters are listed in Table 6 including the numbers for the crystal phase $9Al_2O_3 \cdot 2B_2O_3$.

Finally, Fig. 5 shows the ^{11}B ST MAS spectra of (a) NAB 10, (b) NAB 15 and (c) NAB 20 around the CT region. First of all it is important to note, that the BO_4 and BO_3 ST resonances are completely resolved. There is no overlap between both because of the different quadrupole shift [12, 31]. Besides this, there are only a few MAS ST sidebands for BO_4 reflecting the small coupling constant and a rather large distribution width. Contrary, the ST MAS spinning sidebands for BO_3 can be observed over a frequency range of more than 1.3 MHz on both sides of the CT (Fig-

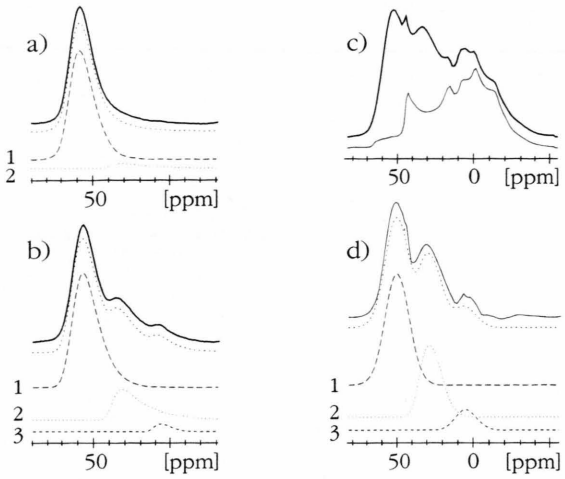

Fig. 4. Comparison between the experimental and analyzed ^{27}Al CT MAS spectra of (a) NAB 10 and (b) NAB 15 at $B_0 = 11.7$ T. The experimental spectrum of NAB 20 at 9.4 T is compared in (c) with the Al spectrum of polycrystalline $9Al_2O_3 \cdot 2B_2O_3$ (bottom spectrum, [17]). The difference of both spectra yields straightforward the NMR lineshape of the remaining glassy matrix. The results of a lineshape fit is shown in (d). 1), 2), and 3) assign $Al(OB)_4$, $Al(OB)_5$, and $Al(OB)_6$ for all samples, respectively.

Table 7. Summary of the ^{11}B ST NMR parameters and assignment of the lines in the NAB glasses.

	δ_{iso} [ppm]	$\Delta\nu$ [Hz]	ν_Q [kHz]	$\Delta\nu_Q$ [kHz]	η	I/I_{total} [%]	Comment
NAB 10	15.9	350	(1290)	100	(0.29)	82.3	BO_3
	+0.3	300	140	80	1.00	17.7	BO_4
NAB 15	14.1	350	1310	50	0.34	86.6	BO_3
	−1.7	300	165	100	0.50	13.4	BO_4
NAB 20	13.6	350	1310	50	0.34	87.6	BO_3 non-ring [33]
	−2.2	300	160	120	0.50	12.4	BO_4

ure 5d). The results of the ST sideband analysis are summarized in Table 7 and Figure 6. With increasing Al_2O_3 content BO_4 units are converted to BO_3 as to be expected. No significant change in the quadrupole interaction parameters is observed, but small changes in the chemical shifts as reported earlier [31]. We would like to mention explicitly, that the analysis of the envelope of the ST MAS sidebands for BO_3 is extremely sensitive. Hence, the mean quadrupole frequency can be estimated with an accuracy of ± 50 kHz, the distribution width with ± 25 kHz and the asymmetry parameter within ± 0.03. We assign

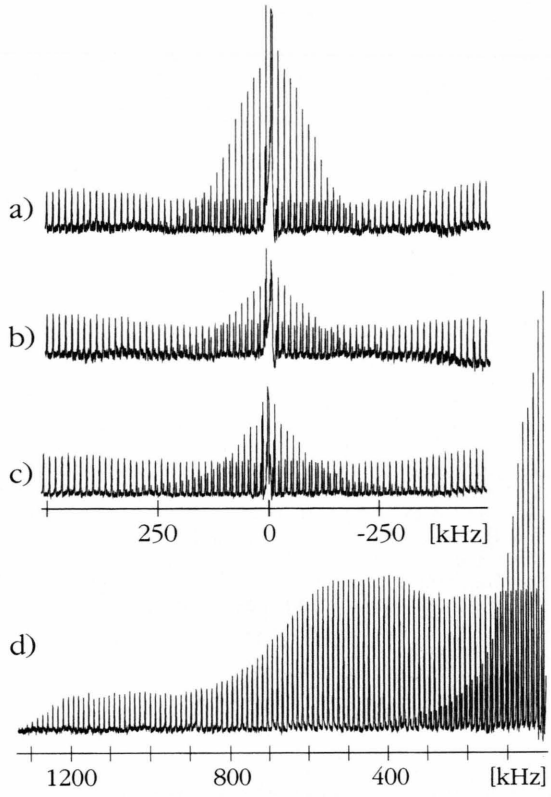

Fig. 5. Experimental ^{11}B MAS NMR spectra of (a) NAB 10, (b) NAB 15 and (c) partially crystallized NAB 20 around the CT region. Note the decrease of the amount of BO_4 between NAB 10 and NAB 15. The left half of the complete ST MAS spectrum is shown for NAB 15 (d). There is a sharp cut off of the spinning sidebands of the ST at about 1.3 MHz, clearly proving a well ordered BO_3 structure. For more details see text.

the BO_3 resonance ($\delta_{iso} = 14$ ppm, $\upsilon_Q = 1.31$ MHz) to a symmetric unit with three bridging oxygens. There is no hint for asymmetric sites.

Interestingly enough, the distribution width for BO_3 is extremely small compared to the mean value. This is obvious from the ST MAS spinning sideband envelopes. Whereas one observes a continuous decrease of the ST MAS spinning sidebands for BO_4 ($\nu_Q = 160$ kHz, $\Delta\nu_Q = 80-120$ kHz), the singularities of the powder pattern are still observable in the BO_3 ST MAS envelope (Figure 5d). This means that the BO_4 units are more distorted than the BO_3 groups. The lineshape simulation for NAB 20 is shown in Figure 6. The ST MAS spinning sidebands between the CT and + 1.1 MHz are shown on the right-hand side in Fig. 6, whereas some of the ST MAS sidebands are

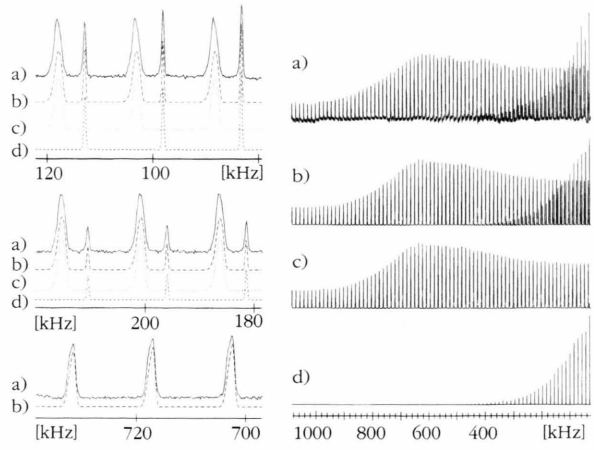

Fig. 6. Comparison of the experimental ^{11}B MAS spectrum and the lineshape simulation of NAB 20. On the right hand side the ST MAS spectrum between the CT region and +1.1 MHz is shown. On the left hand side few ST MAS spinning sidebands taken a different frequencies are shown. The broader lines are the BO_3 resonances, the narrow lines thoses of BO_4 (a), (b), (c), and (d) denote the experimental spectrum, the simulation, the BO_3 and BO_4 resonances in the ST respectively. There is clearly only one BO_3 unit present. See also Results and Outlook sections.

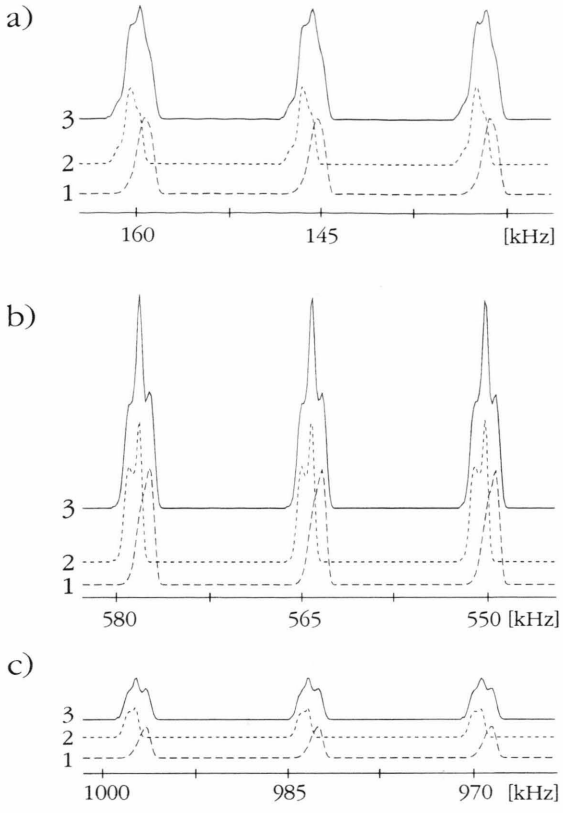

Fig. 7. ^{11}B ST MAS lineshape simulation for the two different BO_3 units of vitreous B_2O_3 for a resonance frequency of 160.46 MHz and an MAS frequency of 14 kHz. The quadrupole and chemical shift data are [32]: 1) $\nu_Q = 1.28$ MHz, $\eta = 0.23$, $\Delta\nu_Q = 100$ kHz, $\delta_{iso} = 13.1$ ppm, (non-ring boron trioxide units); 2) $\nu_Q = 1.34$ MHz, $\eta = 0.21$, $\Delta\nu_Q = 50$ kHz, $\delta_{iso} = 18.1$ ppm; 3) Superposition of the two sites in the ratio 1:1. The distribution widths were chosen according to our experimental results in the ternary glass systems.

plotted on the left-hand side taken at different offsets. The letters a, b, c and d denote the experimental spectrum, the total simulation, the lineshape for BO_3 and BO_4, respectively. The parameters are listed in Table 7. There is clearly only a single type of BO_3 units present. The sharp cut-off of the ST MAS sidebands at about 1.3 MHz (see Fig. 5 d) and the obvious presence of the singularities in the MAS spectra around 500 kHz clearly prove the extremely small distribution width of the quadrupole interaction and the rather constant asymmetry. This is in fact very interesting. Obviously there is only a minor distortion of the BO_3 units in the glass. We conclude, that the network distortions are present mainly in the BO_4, AlO_x, and NaO_x polyhedra, but not in the dominating BO_3 units.

4. Discussion

Phosphate and borate glasses without SiO_2 are interesting for many applications, especially because of their optical properties. Pure P_2O_5 and B_2O_3 can form glasses, but they have low melting points and low T_g. Moreover, these glasses are hygroscopic and contain between 0.05 and 10 wt.% water. Binary $Na_2O-P_2O_5$ and $Na_2O-B_2O_3$ systems form glasses with higher chemical and mechanical stability. But they are not stable enough for practical applications. Adding Al_2O_3 as third component, the stability of these ternary systems increases considerably. Al_2O_3 in combination with P_2O_5 forms very stable glasses but with high melting points (e.g. $Al(PO_3)_3$ with $T_m > 1490\,°C$). However glasses of the binary system $Al_2O_3-B_2O_3$ are not known.

Our aim is to investigate the influence of Al_2O_3 on the glass structure in the two ternary systems $Na_2O-Al_2O_3-P_2O_5$ and $Na_2O-Al_2O_3-B_2O_3$. For our investigations we have chosen a high but constant content of either P_2O_5 or B_2O_3 (70 mole%). The Na_2O/Al_2O_3 ratio was 2, 1, and 1/2.

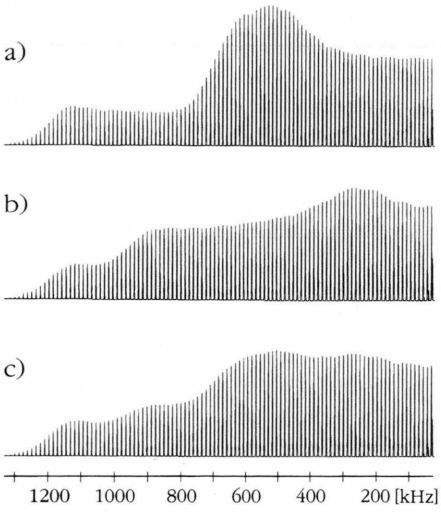

Fig. 8. Simulation of the envelope of the ^{11}B ST MAS lineshape for the two different BO_3 units differing only in the asymmetry parameters (a) $\eta = 0.20$, b) $\eta = 0.60$ with a quadrupole frequency of $\nu_Q = 1.30$ MHz [10] and a distribution width of 50 kHz in order to simulate the glassy structure, c) is the superposition of the two patterns with a ratio 1:1. Even for identical quadrupole frequencies and chemical shifts of both units a separation via the envelope is possible.

In the phosphate glasses we observe a change in the Al coordination number from almost exclusively 6 in NAP 10 to 4, 5, and 6 for the glass NAP 20. But the octahedral coordination of Al still dominates. However, the ^{27}Al MAS spectra also show some minor pentacoordinated Al with phosphorus and octahedrally coordinated Al with Al in NAP 10 and NAP 15. There is no considerable change in the ^{31}P chemical shift, suggesting mainly Q^2 units with possibly different (even mixed) cations. The phosphate based glasses become more stable with decreasing Na_2O/Al_2O ratio. The glass sample NAP 20 could theoretically be $NaPO_3 \cdot 2\,Al(PO_3)_3$, which means a polyphosphate glass with dominating $Al(PO_3)_3$ (Q^2 units) or mixed cation $(Na^+Al^{3+})(PO_3)_4$ structure.

In the borate system we observe a change in the boron coordination number with increasing Al_2O_3 content; more BO_3 units are formed on the expense of BO_4. According to our NMR data ($\delta_{iso} = 14$ ppm, $\nu_Q = 1.31$ MHz), we suggest that these BO_3 units are symmetric, i.e. they have three bridging oxygens. The reasons will be discussed in the next section. Simultaneously, the Al coordination number changes rapidly from 4 (NAB 10) to 4, 5, and 6 for the other glasses. As mentioned earlier, the NAB 20 sample crystallized spontaneously during melting. The main crystal phase is $9\,Al_2O_3 \cdot 2\,B_2O_3$ as detected by X-ray diffraction. This can be quantified by line deconvolution of the NMR spectrum. Nearly 50% of the Al remains in an amorphous phase which mainly contains 4- and 5-coordinated Al units.

5. Outlook: ^{11}B ST Spectroscopy

In this section we want to discuss new aspects and opportunities of ^{11}B ST Spectroscopy. As pointed out in the introduction ^{11}B NMR has been applied to glasses already many years ago. Bray and coworkers have found differences in the quadrupole coupling constants and asymmetry values of the electric field gradient tensors for BO_3 units with only bridging oxygen atoms (symmetric sites, $\eta = 0$, $\nu_Q = 1.3$ MHz) and with one or two terminal oxygen atoms ($\eta = 0.6$, $\nu_Q = 1.3$ MHz) [10] using ^{11}B continuous wave NMR. These findings have been verified recently by NQR [e.g. 33]. Furthermore, 2D DAS NMR spectroscopy has revealed two different BO_3 sites in vitreous B_2O_3 [32] with a difference of 5 ppm in the chemical shifts of boroxol rings and non-ring boron trioxide units by NMR techniques for the first time.

Here we propose ^{11}B ST Spectroscopy as an alternative and simpler technique to tackle this problem. Our approach uses both the ST MAS spectrum obtained at high field (160.46 MHz resonance frequency, $B_0 = 11.4$ T) and high speed MAS (10 ... 15 kHz). There are several reasons for using the high magnetic field strength. Most importantly, the second order quadrupolar broadening of the BO_3 resonances is further suppressed and, simultaneously, the reported chemical shift difference (e.g. 5 ppm [32]) will shift the ST MAS lines of these different BO_3 units against each other. Thus, the difference in the chemical shifts is exploited if various BO_3 sites are present, but the quadrupole interaction can be again recovered from the ST MAS sidebands. In Fig. 7 we compare the positions of the ST MAS lines for the two BO_3 units of vitreous B_2O_3 using the quadrupole and chemical shift data as reported by Youngman and Zwanziger [32]. Obviously, a careful data acquisition should give evidence for the presence of these different units in glasses. For the lineshape calculation we have used distribution widths for the quadrupole interaction as found in our glasses. The straightforward conclusion is, that if chemical shift differences of about 5 ppm are present, different sites can be distinguished simply by inspecting the lineshape of single ST MAS patterns

provided the highest available B_0 field is used. On the other hand one might ask the question what will happen if there are no such large chemical shift differences. So, if only the asymmetry values are different for the two sites, then the ST MAS sideband patterns are quite different even in glasses (see Figure 8). This is due to our astonishing experimental finding, that the distribution width of the quadrupole interaction is rather small (see Result section). Hence even in that case the envelope of the ST MAS sidebands will allow to distinguish between those sites. This is of course the MAS equivalency to cw NMR and certainly, this can be found both in NQR and 2D DAS NMR as well.

The advantages of ^{11}B ST Spectroscopy are straightforward. There are no limitations because of short spin-lattice relaxation nor a necessity to dilute the ^{11}B nuclei which is essential for 2D DAS NMR. With a single experiment at only one B_0 field all relevant parameters can be obtained.

Acknowledgements

C. J. and G. K. F. would like to thank the Deutsche Forschungsgemeinschaft for financial support. It is a real pleasure for one of us (C. J.) to thank Prof. Dr. W. Müller-Warmuth for many interesting discussions and support throughout the past years. We also thank Prof. H. W. Spiess of the Max Planck Institute of Polymer Research in whose laboratory some of the spectra have been acquired.

[1] H. Eckert, Progr. NMR Spectr. **24,** 159 (1992).
[2] G. Engelhard and D. Michel, High-resolution solid-state NMR of silicates and zeolites, John Wiley, Chichester 1987.
[3] R. Dupree, D. Holland, and M. G. Mortuza, J. Non.-Cryst. Solids **116,** 148 (1990).
[4] H. Maekawa, T. Maekawa, K. Kawamura, and T. Yokokawa, J. Non.-Cryst. Solids **127,** 53 (1991).
[5] W. Hater, W. Müller-Warmuth, M. Meier, and G. H. Frischat, J. Non.-Cryst. Solids **113,** 210 (1989).
[6] J. Stebbins, J. Non.-Cryst. Solids **106,** 359 (1988).
[7] A. R. Grimmer, M. Mägi, M. Hähnert, H. Stade, A Samoson, W. Wieker, and E. Lippmaa, Phys. Chem. Glasses **25,** 105 (1984).
[8] P. Losso, B. Schnabel, C. Jäger, U. Sternberg, D. Stachel, and D. O. Smith, J. Non.-Cryst. Solids **143,** 256 (1992).
[9] A. H. Silver and P. J. Bray, J. Chem. Phys. **29,** 984 (1958); S. G. Bishop and P. J. Bray, Phys. Chem. Glasses **7,** 73 (1966).
[10] P. J. Bray, S. J. Gravina, P. H. Hintenlang, and R. V. Mulkern, Magn. Reson. Rev. **13,** 263 (1988).
[11] D. Müller, I. Grunze, E. Hallas, and G. Ladwig, Z. Anorg. Allg. Chem. **500,** 80 (1983).
[12] C. Jäger, Satellite Transition Spectroscopy of Quadrupolar Nuclei NMR – Basic Principles and Progress, Vol. **31,** 135 (1994).
[13] C. Jäger, Dupree, S. C., Kohn, and M. G. Mortuza, J. Nonc-Cryst. Solids **155,** 95 (1993).
[14] C. Jäger, J. Magn. Reson. **99,** 353 (1992).
[15] C. Jäger, W. Müller-Warmuth, C. Mundus, and L. van Wüllen, J. Non.-Cryst. Solids **149,** 209 (1992).
[16] C. Jäger, G. Kunath, P. Losso, and G. Scheler, Solid State Nucl. Magn. Reson. **2,** 73 (1993).
[17] G. Kunath, P. Losso, S. Steuernagel, H. Schneider, and C. Jäger, Solid State Nucl. Magn. Reson. **1,** 261 (1992).
[18] M. E. Smith, C. Jäger, R. Schönhofer, and S. Steuernagel, Chem. Phys. Lett. **219,** 75 (1994).
[19] G. Kunath-Fandrei, T. Bastow, C. Jäger, and M. E. Smith, in press: Chem. Phys. Letters.
[20] G. Kunath-Fandrei, P. Rehak, H. Schneider, and C. Jäger, Solid State Nucl. Magn. Reson. **3,** 241 (1994).
[21] H. J. Jakobsen, J. Skibstedt, H. Bildsøe, and N. C. Nielsen, J. Magn. Reson. **85,** 173 (1989).
[22] N. C. Nielsen, H. Bildsøe, and H. J. Jakobsen, Zeolites **11,** 622 (1991).
[23] J. Skibstedt, H. Bildsøe, and H. J. Jakobsen, J. Magn. Reson. **92,** 669 (1991).
[24] J. Skibstedt, N. C. Nielsen, H. Bildsøe, and H. J. Jakobsen, J. Magn. Reson. **95,** 88 (1991).
[25] J. Skibstedt, N. C. Nielsen, H. Bildsøe, and H. J. Jakobsen, Chem. Phys. Lett. **188,** 405 (1992).
[26] J. Skibstedt, E. Henderson, and H. J. Jakobsen, Inorg. Chem. **32,** 1013 (1993).
[27] D. Massiot, A. Kahn-Harari, D. Michel, D. Müller, and F. Taulelle, Magn. Reson. Chem. **28,** S82 (1990).
[28] F. Taulelle, C. Bessada, and D. Massiot, J. Chem. Phys. **89,** 379 (1992).
[29] D. Massiot, C. Bessada, J. P. Coutures, and F. Taulelle, M. Magn. Reson. **90,** 231 (1990).
[30] L. B. Alemany, D. Massiot, B. L. Sherriff, M. E. Smith, and F. Taulelle, Chem. Phys. Lett. **177,** 301 (1991).
[31] L. van Wüllen and W. Müller-Warmuth, Solid State Nucl. Magn. Reson. **2,** 279 (1993).
[32] R. E. Youngman and J. W. Zwanziger, J. Non.-Cryst. Solids **168,** 293 (1994).
[33] S. J. Gravina and P. J. Bray, Z. Naturforsch. **45a,** 268 (1990).
[34] J. Herzfeld and A. E. Berger, J. Chem. Phys. **73,** 6021 (1980).
[35] U. Haubenreiser, Dissertation B, FSU Jena 1985.
[36] R. K. Brow, C. C. Phifer, G. L. Turner, and R. J. Kirkpatrick, J. Amer. Ceram. Soc. **74,** 1287 (1991).
[37] I. L. Mudrakovski, V. P. Shmachkova, N. S. Kotsarenko, and V. M. Mastikhin, J. Phys. Chem. Solids **47,** 335 (1986).
[38] S. Hayashi and K. Hayamizu, Bull. Chem. Soc. Japan **62,** 3061 (1989).
[39] D. Ehrt and C. Jäger, Z. Phys. Chem. **162,** 97 (1989).
[40] R. K. Brow, R. J. Kirkpatrick, and G. L. Turner, J. Amer. Ceram. Soc. **73,** 2296 (1990).
[41] B. C. Bunker, R. J. Kirkpatrick, R. K. Brow, G. L. Turner, and C. Nelson, J. Amer. Ceram. Soc. **74,** 1425 (1991).
[42] D. Müller, I. Grunze, E. Hallas, and G. Ladwig, Z. Anorg. Allg. Chem. **500,** 80 (1983).
[43] M. A. Fedotov, I. L. Mudrakovskii, V. M. Mastikhin, and V. P. Shmachkova, Izv. Akad. Nauk SSSR, Ser. Khim. (Engl. Transl.) **10,** 2169 (1988).